

In-situ fabrication of TiC-Al₂O₃ and TiB₂-TiC-Al₂O₃ composite coatings on 304 stainless steel surface using GTAW process

E. Bahramizadeh, S. Nourouzi, H. Jamshidi Aval*

Department of Materials Engineering, Babol Noshirvani University of Technology, Shariati Ave., Babol 47148-71167, Iran

Received 27 July 2018, received in revised form 9 March 2019, accepted 20 March 2019

Abstract

The purpose of this study was to improve the performance of 304 stainless steel by applying a wear-resistant coating. For this purpose, in-situ composite coatings of TiC-Al₂O₃, as well as TiB₂-TiC-Al₂O₃, were applied on the surface of 304 stainless steel by using combining, welding and self-combustion synthesis with different current welding. The microstructural investigations of the coated layers showed that due to the high incoming welding temperature in all the samples, by performing the combustion synthesis reaction, significant reinforcing particles were formed on the 304 stainless steel surface. Also, in all heat inputs, cubic titanium carbide particles formed inhomogeneously on Al₂O₃ particles or spontaneously in the austenitic matrix of 304 stainless steel. The reinforcing of TiC and TiB₂ particles formation in both 3TiO₂-4Al-3C and 3TiO₂-4Al-B₄C layers led to an increase in surface hardness and wear resistance up to 2.5 versus the substrate.

Key words: gas tungsten arc welding (GTAW), composite, 304 stainless steel, microstructure

1. Introduction

Considering the mechanical properties, corrosion resistance, and cost efficiency of austenitic stainless steels, they are commonly used in industries. Nevertheless, in many applications, they exhibit low surface hardness and inadequate wear resistance [1, 2]. AISI 304 stainless steel is known to have low wear resistance and hardness, given its specific features, including proper machinability and aqueous corrosion resistance [3]. Consequently, we can use surface treatments for improving the surface properties of this type of steel. There are mainly two available techniques to combine reinforcement particles in the matrix of MMCs. One is solid state processing, and the other technique is an in-situ organization of the reinforcement phase within the matrix of material [4]. The main fabrication methods for solid-state processing of metal matrix composites are powder blending and consolidation. In-situ reinforced coatings are considered more useful, given proper reinforcement matrix interfaces and thermodynamic stability in the matrix in comparison with

external additives. The reinforced particles are also finer in size and their distribution in the matrix of the substrate is even more uniform [5]. A cost-effective approach is an application of wear-resistant and hard coatings via weld deposition from different alloys or metals on metallic substrates, particularly for expensive and large components. The coatings are deposited as thick alloy coatings via weld deposition, ranging from 750 μm to a few mm in size [6].

The gas tungsten arc welding (GTAW) process is recognized as the most convenient surface modification method that allows preparation of crack-free samples in coating layers and good metallurgical properties at the interface between the coated layer and substrate [7]. Given their great stiffness, toughness, high specific strength, and high wear resistance, major attention is being directed towards metal matrix composites (MMCs) reinforced by ceramic. These composites are also associated with low costs of fabrication, adequate high-temperature stability, and desirable isotropic features [8]. They may also be applied as high-temperature structural compounds and wear-

*Corresponding author: tel.: +98 11 35501808; fax: +98 11 35501802; e-mail address: h.jamshidi@nit.ac.ir

resistant parts. TiC, TiB₂, and Al₂O₃, as ceramic particulates, exhibit great hardness, and adequate chemical and thermal stability, excellent wear resistance, and high melting points. Therefore, they can be potential compounds for incorporation in multi-component coatings to enhance resistance to mechanical and thermal wear [9].

Due to low energy consumption and high purity of products, self-propagation high-temperature synthesis (SHS), as one of the techniques of the synthesis of reinforcing ceramic particles, has attracted the attention of many researchers [10]. Recently, various studies have concentrated on (TiC-Al₂O₃)/Al and (TiB₂-Al₂O₃)/Al reaction synthesis in Al-TiO₂-X systems (X is B, C, or B₂O₃) [11]. In recent years, several research groups have shown interest in GTAW coating/alloying by using TiC as reinforcement on various substrate materials like 1020 steel [12], AISI4340 [13], AISI304, and 1020 [14]. Chatterjee et al. [13] integrated the SHS and the laser-welding processes to coat Al₂O₃-TiB₂-TiN composite on the surface of soft steel. Hou et al. [15] used the Al-TiO₂-B₂O₃ reaction system and plasma-cladding process to make a composite coating on the surface of Q235A steel. Nam

et al. [14] studied on TiC-Al₂O₃ and (Ti,W)C-Al₂O₃ ceramic reinforced MMC fabricated by gas tungsten arc cladding. They found that the reinforced particles formed by the in-situ reaction were maintained at a smaller size than the original particles. Sharifitabar et al. [16] investigated the fabrication of Fe-TiC-Al₂O₃ composites on the surface of steel using a TiO₂-Al-C-Fe combustion reaction induced by gas tungsten arc cladding. They show that this composite substantially improves the substrate hardness. Mastana et al. [17] studied the microstructure and properties of TiB₂-TiC-Al₂O₃ coating prepared by laser-assisted SHS and subsequent cladding with micro-/nano-TiO₂ as precursor constituent. They reported that nano-size TiO₂ improves the hardness and wear resistance of the coating. Cai et al. [18] studied the influence of CeO₂ on tribological behavior of TiC/Fe-based composite coating. They found that the micro-hardness and wear properties of the cladding layer had a close relationship with the shape, size, distribution, and the form of TiC ceramic particles.

For the first time, this study investigates in-situ TiC-Al₂O₃ and TiB₂-TiC-Al₂O₃ composite fabrication using the GTAW process to increase the wear

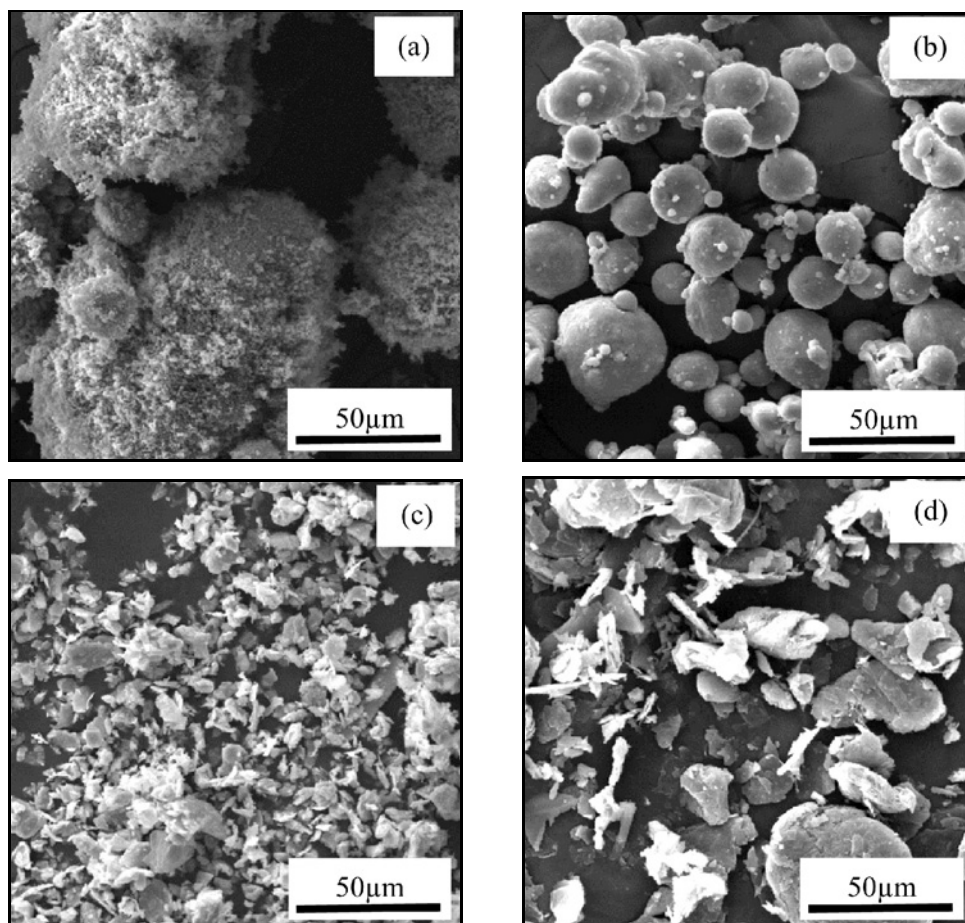


Fig. 1. SEM micrograph of powders: (a) TiO₂, (b) Al, (c) B₄C, and (d) C.

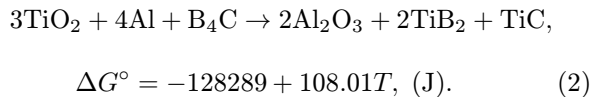
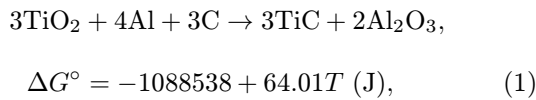
Table 1. Chemical composition of mixtures used during coating (wt.%)

Mix	TiO ₂	Al	C	B ₄ C
1	62.50	28.12	9.38	–
2	59.45	26.79	–	13.76

resistance and hardness of AISI304 stainless steel. Finally, the microstructural features and the phase characterization of the coated samples were investigated by using optical and electron microscopy and X-ray diffraction analysis. The mechanical properties of coated layers were studied by Vickers microhardness and pin-on-disk wear tests.

2. Experimental procedure

A sample of 304 stainless steel, measuring 130 mm × 30 mm × 5 mm, was used as the substrate material. It contained 0.04 C, 0.52 Si, 18.50 Cr, and 8.00 Ni. The powders used as reactants in the present study were TiO₂, Al, C, and B₄C with an average particle size of 1, 20, 20, and 10 μm, respectively. The morphology of the powders is shown in Fig. 1. The component ratios of the mixer (1) and mixer (2) are listed in Table 1. To probe the feasibility of self-propagation synthesis by gas tungsten arc welding, the prediction of thermodynamic oxidation of metal oxide by aluminum was investigated separately for both powdery compositions. A study by Merzhanov [19] proved that for self-propagation synthesis, the calculated adiabatic temperature in chemical reactions should be above 1800 K. In most researches, this temperature is known as the Merzhanov criterion. The adiabatic temperatures obtained for reactions by Eqs. (1) and (2) were 2390 and 2423 K, respectively. Therefore, both reactions have the ability to advance.



The two-step method was applied for coating. To remove machining marks, an emery paper was used for polishing the surface of the specimen. Following milling with a ball-milling machine, polyvinyl alcohol (4 wt.%) was used to blend the mixed powder; then, the mixture was agitated for paste formation. The paste was deposited on the AISI-304 stainless

Table 2. The coating process parameters

Sample code	Current (A)	Heat input (kJ mm ⁻¹)	Welding speed (mm s ⁻¹)
S1,T1	100	1.6	1.1
S2,T2	120	1.9	1.1
S3,T3	140	2.3	1.1

steel substrate surface to a thickness of 0.8 mm. The coated substrate was then dried at 100 °C in a furnace for 1 hour to remove moisture. Table 2 presents the parameters.

The coating was achieved using a GTAW torch. For this purpose, a 2 % thoriated tungsten electrode was used (nozzle diameter, 6 mm). To provide an inert environment and prevent oxidation, argon (flow rate, 10 l min⁻¹) was directly blown to the molten pool, as well as the coating-processing site. According to Table 2, to achieve the most favorable mechanical properties, samples with different welding currents were used in both powder compositions. The samples coated by mixed powders (TiO₂, Al, C) and (TiO₂, Al, B₄C) were named by the letters “S” and “T”, respectively. After applying the coated layers on the substrate surfaces, for microstructure studies of the coated layers, due to the fact that the reinforcing phases were not visible in the coated layers with optical microscopy, scanning electron microscope (SEM) equipped with elemental analysis by energy dissipation spectrophotometry was used to determine the elements formed and to provide the elemental analysis of the phase particles at the surface substrates and their distribution. To determine the formation of phases in the coated layers, X-ray diffraction analysis was used. The microhardness of the samples was measured by using a 100 g load for 10 s. Also, a pin-on-disk wear test was used to examine the wear properties of the coatings. The pin was held against the counter face of a rotating disk with wear track diameter 100 mm. The disk was made of the steel hardened up to HRC 63 with a diameter of 50 mm. The wear test for all specimens was conducted under the normal loads of 10 N, with a sliding speed of 60 rpm and at a distance of 250 m.

3. Results and discussion

The amount of heat input applied to the workpiece affects the microstructure, penetration, and shape of the weld region. The macrostructures of the coated samples are presented in Fig. 2. As it is evident, in both the reaction powder samples (S1, S2, S3, T1, T2, and T3), by increasing the heat input from samples S1 to S3 and T1 to T3, the width and the penetration depth of the coated layer increased. Table 3 shows the

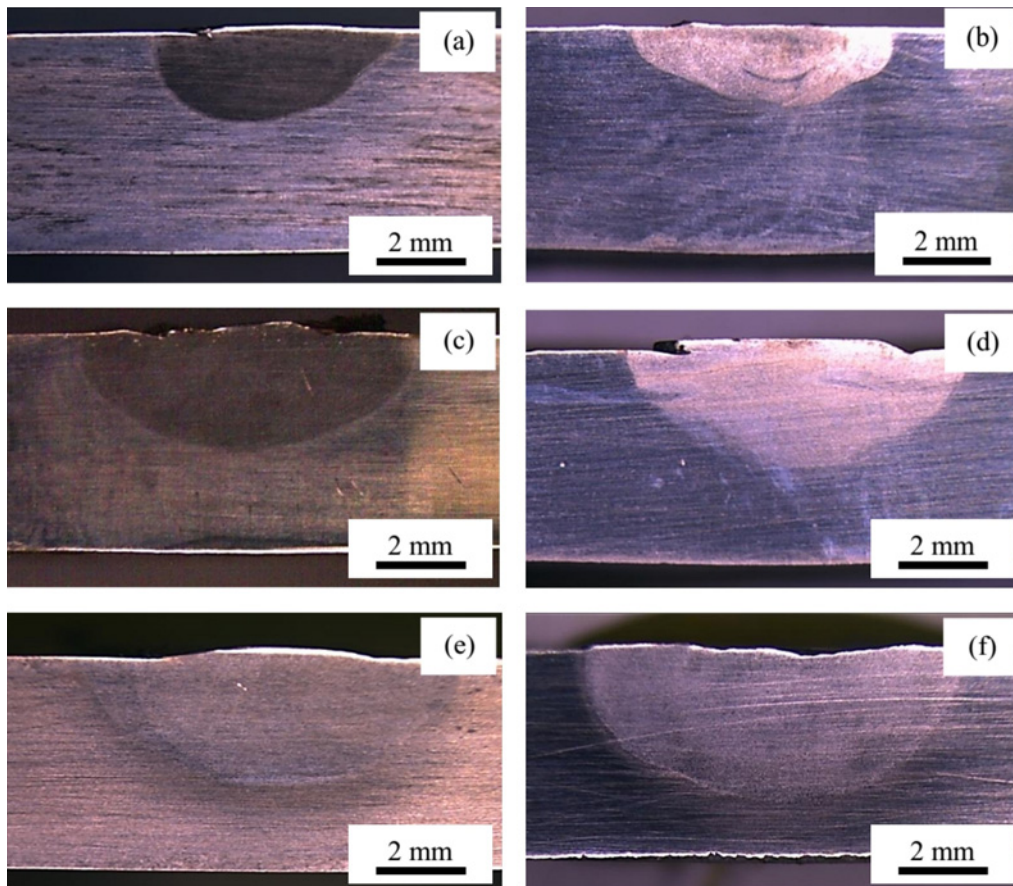


Fig. 2. Macrostructures of the coated samples: (a) sample S1, (b) sample T1, (c) sample S2, (d) sample T2, (e) sample S3, and (f) sample T3.

Table 3. Effect of heat input on the width and penetration depth of weld

Sample code	Heat input (kJ mm)	Weld width (mm)	Penetration depth (mm)
S1	1.6	~ 6	~ 2
S2	1.9	~ 8	~ 2.8
S3	2.3	~ 9	~ 3
T1	1.6	~ 6.5	~ 2
T2	1.9	~ 8	~ 3
T3	2.3	~ 9	~ 3.5

approximate value of the width and the penetration depth of the coated layer measured for the S1, S2, S3, T1, T2, and T3 samples.

Figure 3 shows the different weld zones of the sample S2. Figures 3b,c show the variation of δ -ferrite morphology in the fusion zone of sample S2. It is clear that two different kinds of lathy δ -ferrite and skeletal δ -ferrite were formed in the austenite matrix of sample S2. Similar δ -ferrite morphologies were observed in the fusion zone of all the coated samples. This phenomenon is dependent on various thermal cycles and

cooling rates in the welding zone. Where the cooling rates were moderate, skeletal δ -ferrite morphology was formed. This was attributed to the advances of ferrite-consuming austenite before ferrite was adequately enriched in ferrite-promoting elements (e.g., chromium) and depleted in austenite-promoting elements (e.g., nickel); in case of limited diffusion, it showed stability at lower temperatures. However, at high cooling rates, a lathy δ -ferrite morphology was formed [20, 21]. Since the cooling rate is higher in the welding center than the other welding zones, a lathy δ -ferrite was formed. A skeletal δ -ferrite was formed as far as the weld center and near the interface of the coated layer and the base metal due to lower cooling rates. Figure 3c shows the skeletal ferrite. The lathy morphology was formed due to restricted diffusion during the ferrite-austenite transformation. Decreasing the diffusion distances increased the efficiency of the transformation to proceed and therefore decreased the spaced laths [15].

Figure 3d shows the interface between the weld metal and the substrate, which is austenitic stainless steel. An epitaxial growth in this region was observed for all the coated samples (S1, S2, S3, T1, T2, and T3). This type of growth is useful for connecting the grain of the weld zone to the base metal and prevents

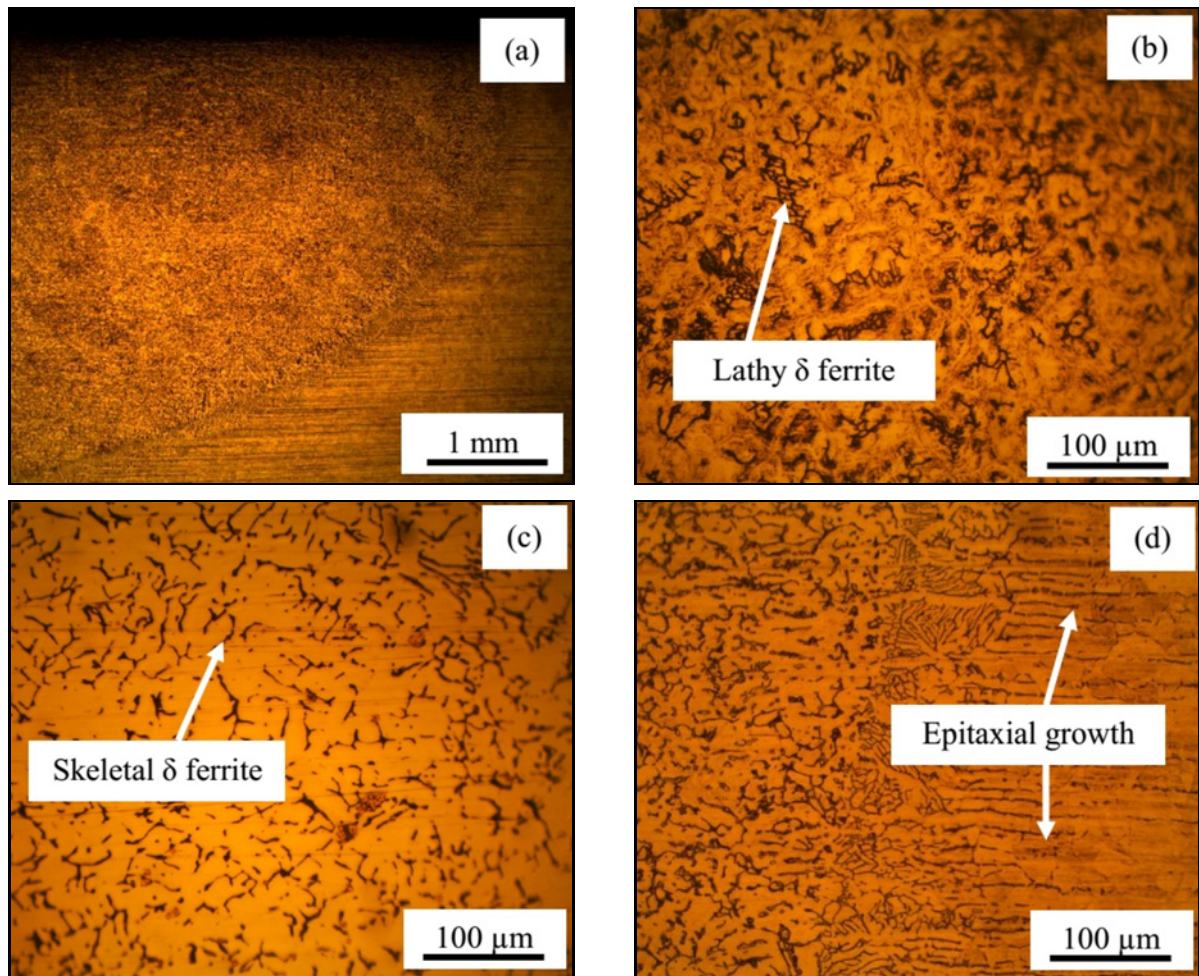


Fig. 3. Microstructure of (a) welding zone, (b) center of coated layer (zone A), (c) near the interface of coated layer and base metal (zone B), and (d) interface of coated layer and base metal of sample S2 (zone C).

the concentration of stress in the weld and the heat-affected zones. One of the main characteristics of this growth is the similarity of the crystalline structures and the chemical compositions of the weld metal and the base metal, which can prevent the formation of stress in the joint [21, 22].

Figure 4 shows the X-ray diffraction pattern prepared from the surface of the samples S1, S2, and S3. In all the coated samples in reaction 1 ($3\text{TiO}_2\text{-4Al-3C}$), the combustion synthesis was carried out on the surface of the coating layer due to the high temperature of the welding, which resulted in the formation of significant reinforcement phases on the coated surfaces. According to Fig. 4, the X-ray diffraction pattern related to the surface of the coating layer includes two high-intensity peaks that are related to austenite and δ -ferrite and two low-intensity peaks, which indicate the TiC and Al_2O_3 phases on the surface. The TiC- and Al_2O_3 -phase peaks indicated that due to the reaction of combustion in $3\text{TiO}_2\text{-4Al-3C}$ powder mixture, significant heat was produced due to Al and TiO_2 reactions [23]. As previously said, the adiabatic

temperature obtained to produce the $\text{TiC-Al}_2\text{O}_3$ ceramic is 2390 K. This temperature is higher than the calculated adiabatic temperature 1800 K in chemical reactions for self-propagation synthesis. Therefore, reactions to produce the $\text{TiC-Al}_2\text{O}_3$ have the ability to advance. The reaction is initiated by a reaction between TiO_2 and aluminum. The sequence of reactions is thought to be, the aluminum phase melts and reacts with the TiO_2 , and the titanium reacts with the free carbon to produce the $\text{TiC-Al}_2\text{O}_3$ ceramic.

The microstructures of the center of the coated layers in the samples S1, S2, and S3 are shown in Fig. 5. In all the samples, titanium carbide particles were mainly formed with cubic morphology. For all the samples, these particles are indicated with the circle mark in Fig. 5. The approximate average volume per cent of titanium carbide in the coated layers of S1, S2, and S3 were 4.51, 4.97, and 3.87, respectively. Therefore, sample S2 is most suitable for welding parameters. Figure 6 shows the particle size of the titanium carbide in the coated layer of the sample S2. According to the SEM micrograph, the maximum

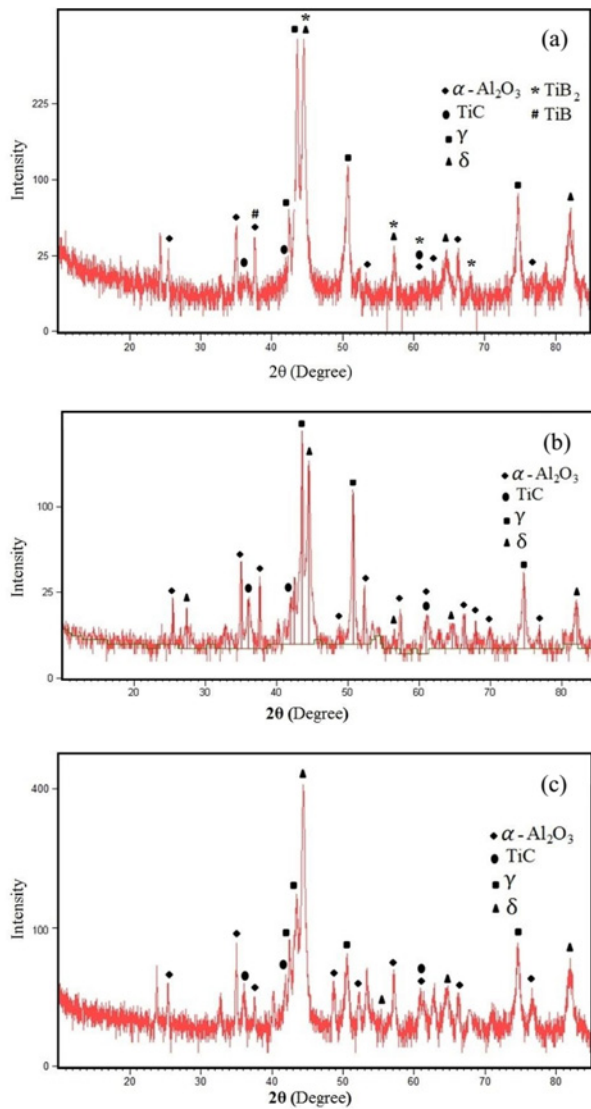


Fig. 4. X-ray diffraction pattern of the samples: (a) S1, (b) S2, (c) S3.

size of cube-shaped particles was $3.31 \pm 0.35 \mu\text{m}$. According to Fig. 7a, a dark point was observed in the center of some particles of the primary titanium carbide. Some primary titanium carbide particles were non-homogeneously formed on Al_2O_3 particles. Given that the free energy of the formation of Al_2O_3 was less than that of TiC at the same temperature, fine particles of Al_2O_3 were formed in the early stages of nucleation and remained in the melt. When there are enough elements to form the titanium carbide in the melt, aluminum oxide can act as the preferred primer for non-homogeneous titanium carbide nucleation [9, 24, 25]. Figures 7b,c show the EDS analyses of TiC and Al_2O_3 particles in Fig. 7a. Due to the lightness of oxygen, carbon, and boron, as well as their inability to be identified under an electron microscope, it can be said that the titanium-rich particles are titanium

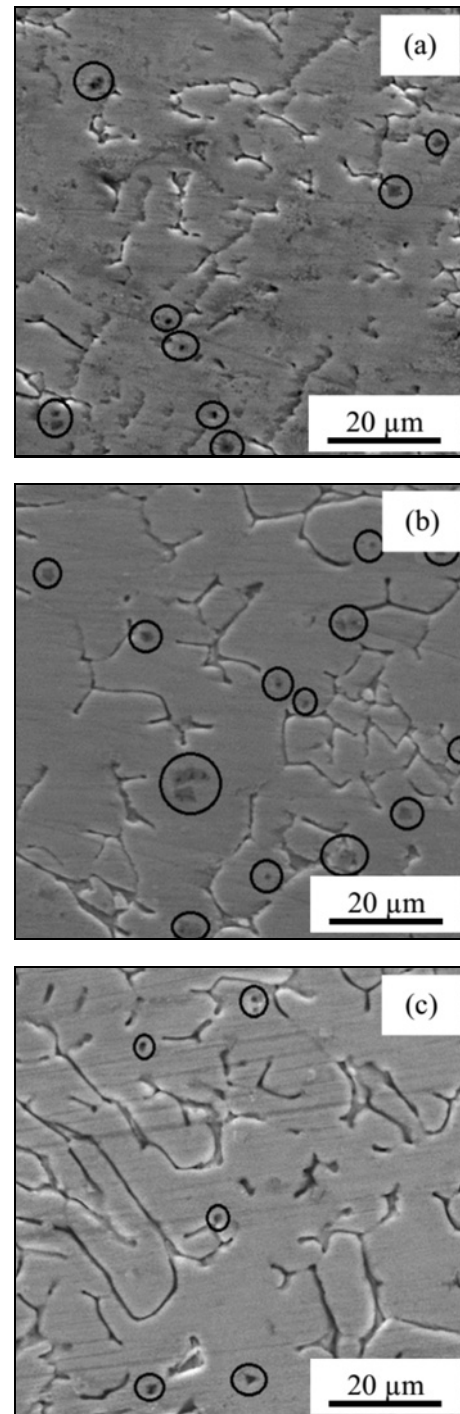


Fig. 5. SEM micrograph of coated layer of: (a) S1, (b) S2, (c) S3.

carbide. Also, the cubic particle center was rich in aluminum, indicating the presence of Al_2O_3 at the TiC center (non-homogeneous TiC nucleation on Al_2O_3).

TiB_2 is characterized by high chemical and thermal stability up to 1700°C , great hardness, high melting point, good wear resistance, and high strength-to-density ratio [26]. Therefore, for the second sample,

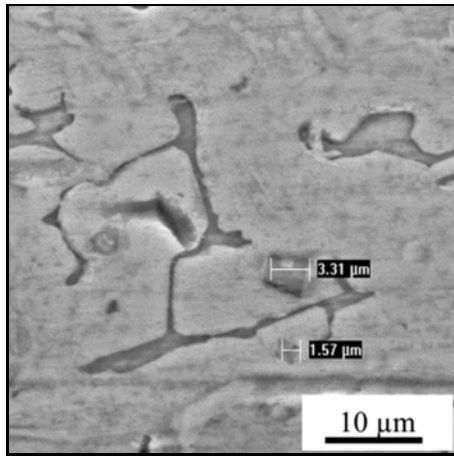
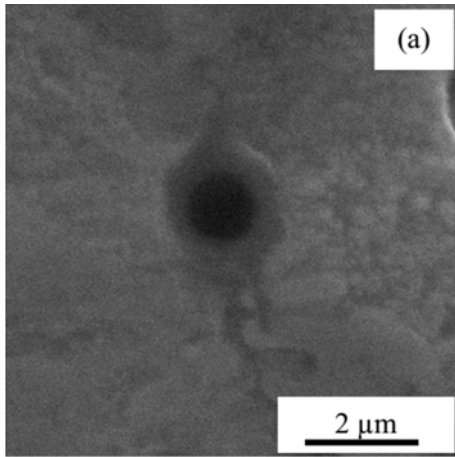


Fig. 6. TiC particle size in a matrix of sample S2.



(a)

Element	Ti	Fe	Al	Cr	Ni
Content / wt%	64.23	16.21	12.61	4.32	2.63

(b)

Element	Ti	Fe	Al	Cr	Ni
Content / wt%	12.15	5.23	71.01	7.13	4.48

Fig. 7. (a) SEM micrograph of TiC and Al₂O₃ particles in sample S2, (b) EDS analysis of TiC, and (c) EDS analysis of Al₂O₃.

a 3TiO₂-4Al-B₄C powder mixture was used to form a TiB₂-TiC-Al₂O₃ composite coating on the 304 stainless steel surface. Figure 8 presents the X-ray diffraction (XRD) spectra of T1, T2, and T3 coated layers. The phases in the coatings were detected as TiC, TiB₂, and Al₂O₃ after GTAW melting. Therefore, in the austenite matrix of 304-stainless steel, it is possible to synthesize a mixture of multiple TiC-TiB₂-Al₂O₃ ceramic phases in situ.

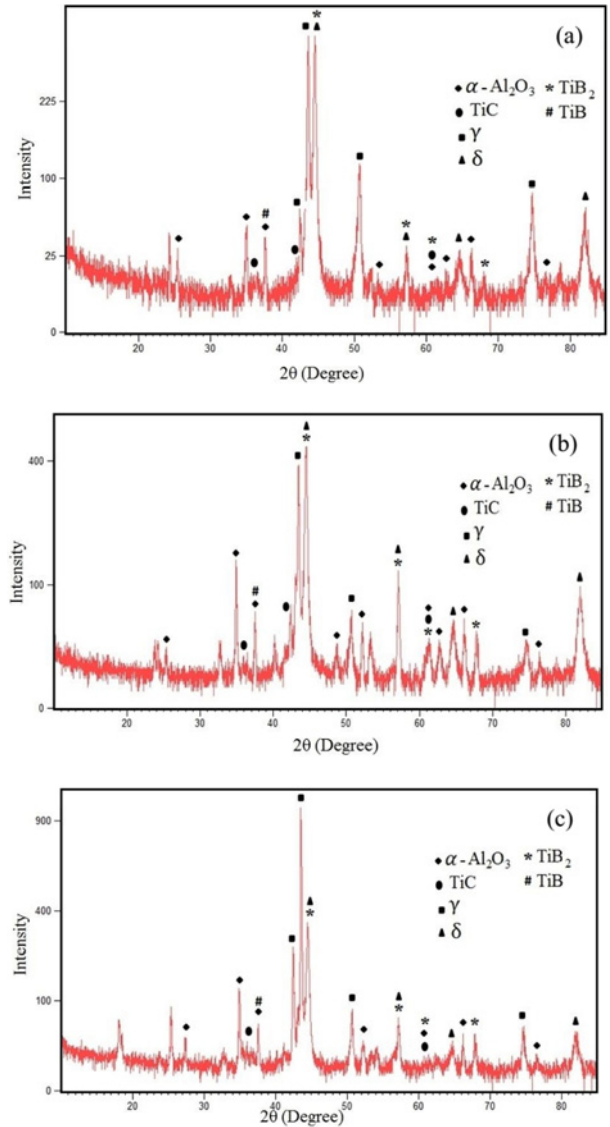


Fig. 8. The X-ray diffraction pattern of the samples: (a) T1, (b) T2, and (c) T3.

Solid-liquid reactions, solution precipitation, and solid-solid interface reactions may be the mechanisms involved in TiB₂ and TiC reinforcement in situ in the stainless steel matrix [27]. The liquid phase exists at 1130 and 1174 °C in Fe-Ti-C and Fe-Fe₂B systems, respectively. During the solid-liquid reaction first, the nucleation of the TiC occurs via titanium diffusing into the carbon and precipitating out as carbide via a solid-liquid reaction (above 1130 °C). Second, the TiB₂ reinforcements are formed when the liquid melt in Fe-Fe₂B system surrounds the Ti powder particles, and TiB₂ occurs via boron diffusing into the Ti and precipitating out as a boride via solid-liquid reaction (above 1174 °C). Thus, the liquid metal phase favors the solid-liquid interface reactions. The TiC and TiB₂ combination was stable thermody-

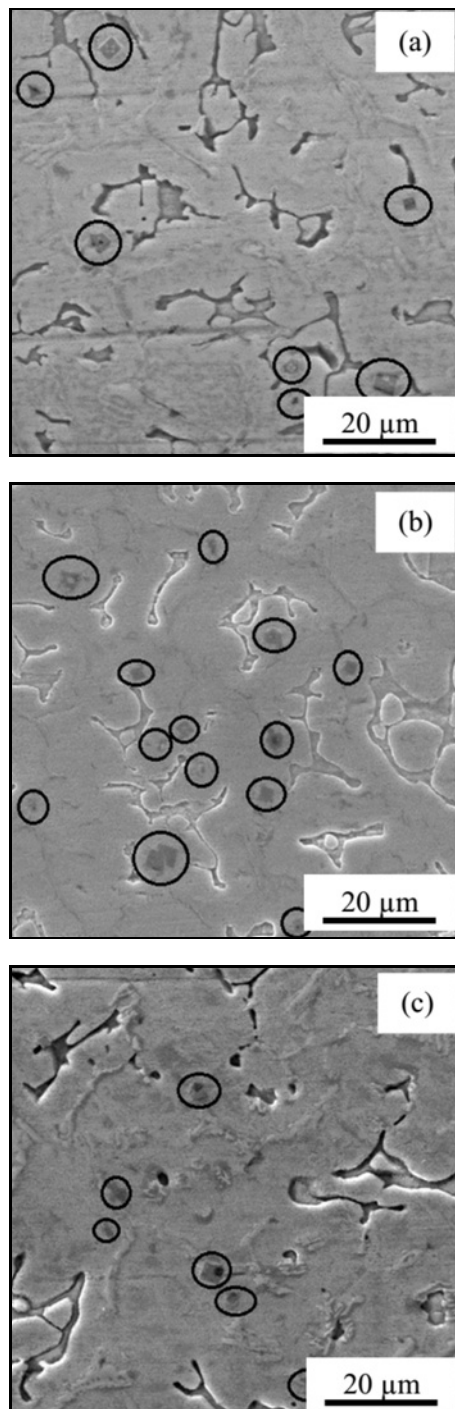
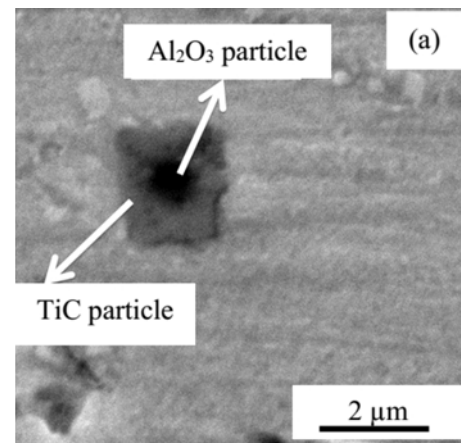


Fig. 9. SEM micrograph of the coated layer of: (a) T1, (b) T2, and (c) T3.

namically up to 2600°C at which point a pseudo binary eutectic reaction was found [28]. In other words, the first reaction in the $3\text{TiO}_2\text{-4Al-B}_4\text{C}$ powder mixture was the reaction of Al with TiO_2 , which led to the extraction of Ti from its oxide. Owing to greater diffusion of C than B, C first reacts rapidly with Ti and TiC is formed. Then the released B reacts with



(a)

Element	Ti	Fe	Al	Cr	Ni
Wt%	68.21	18.12	8.23	3.14	2.30

(c)

Element	Ti	Fe	Al	Cr	Ni
Wt%	10.32	4.32	77.30	6.23	1.83

Fig. 10. (a) SEM micrograph of TiC and Al_2O_3 particles in sample T2, (b) EDS analysis of TiC, and (c) EDS analysis of Al_2O_3 .

the remaining Ti, and in the austenite matrix of 304 stainless steel, it is formed as the TiB_2 or TiB phase [28]. The microstructures of the coated layers in the T1, T2, and T3 samples are shown in Fig. 9. Like in the first powder reaction, titanium carbide particles were mainly formed with cubic morphology in each of the coatings in this powder reaction as well. For all the samples (T1, T2, and T3), these particles are indicated with a circle mark in Fig. 9. The approximate average volume per cent of titanium carbide in the coated layers of T1, T2, and T3 was 4.13, 5.21, and 2.42, respectively. Therefore, the heat input used in sample T2 was found to be most suitable due to the formation of a higher amount of reinforcement particles.

Figure 10a shows one of the particles in the austenite matrix that is shown at a larger magnification. In this figure, the gray particle marked with the arrow shows the TiC particle. Figure 10b presents the EDS analysis of the TiC particle. The black particle indicated by an arrow in Fig. 10b is the Al_2O_3 particle. Figure 10c presents the EDS analysis of Al_2O_3 . The TiB_2 phase was not detectable in the electron microscopic images of the coating layer. Therefore, to demonstrate the existence of this phase, we could see the analysis of the diffraction pattern from the surface of the coated layer. Figure 11 shows the gray particle EDS analysis in the coated layer of sample T2. It con-

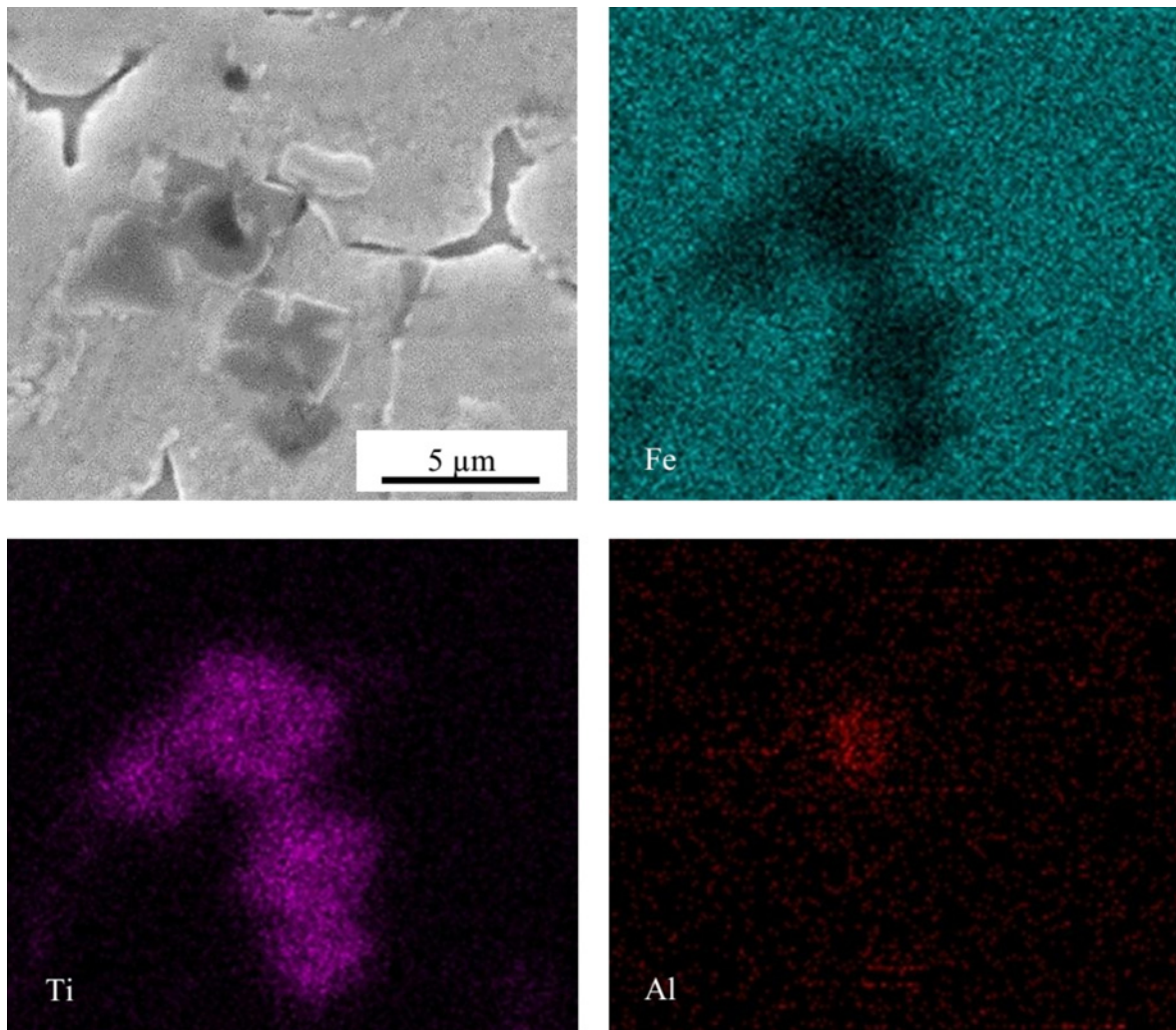


Fig. 11. Element mapping results in the coated layer of sample T2.

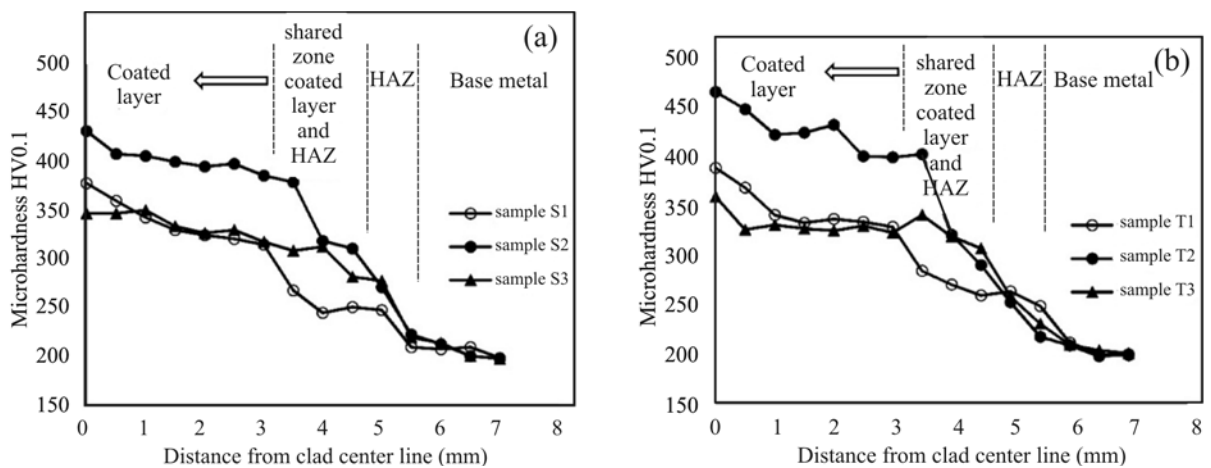


Fig. 12. The hardness distribution profile of (a) sample S1, S2, and S3 and (b) samples T1, T2, and T3.

sists of Ti, while high Fe concentrations are found in the matrix; Al concentration is insignificant in these phases.

Figure 12 shows the variation in the hardness of

the different welding areas in the coated samples. The hardness was measured at a depth of 200 μm from the surface of the base metal. According to the hardness profile illustrated in Fig. 12a, due to the formation of

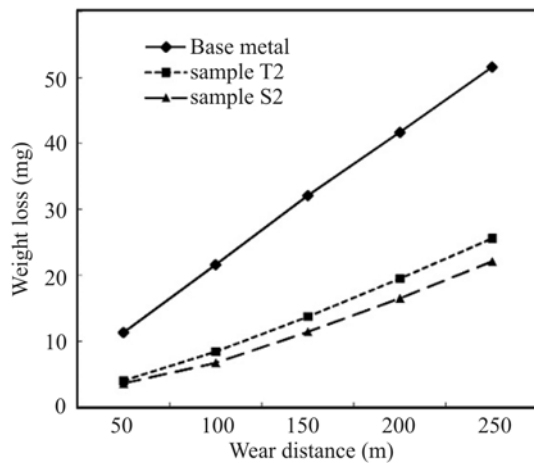


Fig. 13. Weight loss of base metal and samples S2 and T2.

TiC-Al₂O₃ composites in the coated layers, the hardness of 304 stainless steel substrate (about 198 HV) increased in the coated samples (332, 383, and 315 HV for samples S1, S2, and S3, respectively). Therefore, the most optimal welding parameters for coating were in sample S2, which in terms of microstructure and the rate of reaction were produced by the combustion synthesis, produced the most hardness on the steel surface. Figure 12b shows the hardness distribution profile in the T1, T2, and T3 samples. In this sample, a composite coating of TiC-Al₂O₃-TiB₂ was formed on the surface due to the change in the composition and use of B₄C powder in the powder composition as the carbon source. The formation of the composite coating on the surface of the specimens increased the hardness of the T1, T2, and T3 samples to 350, 421, and 326 HV, respectively. The difference in hardness between samples S2 and T2 was due to the presence of TiB₂ in the coating layer. It could be seen that in both mixtures, with increasing heat input, the hardness first increased and then decreased. According to Figs. 4 and 8, reinforcement particles were formed under all conditions, but with increased heat input, the dilution increased, and the reinforcement volume per cent decreased.

Since the coated samples of S2 and T2 had higher hardness, these samples were selected to examine the wear behavior and comparison with the 304 stainless steel substrate. Figure 13 shows the weight loss in the coated and substrate samples after the wear test. The improvement in the wear behavior of the samples was directly related to their hardness. Under the same conditions, the coated samples' wear behaviors were nearly 2.5 times that of the austenitic 304-stainless steel substrate. Considering the presence of reinforcing particles (e.g., TiC-Al₂O₃ on the coated surface of sample S2 and TiC-Al₂O₃-TiB₂ on the surface of sample T2) because of the higher surface hardness and

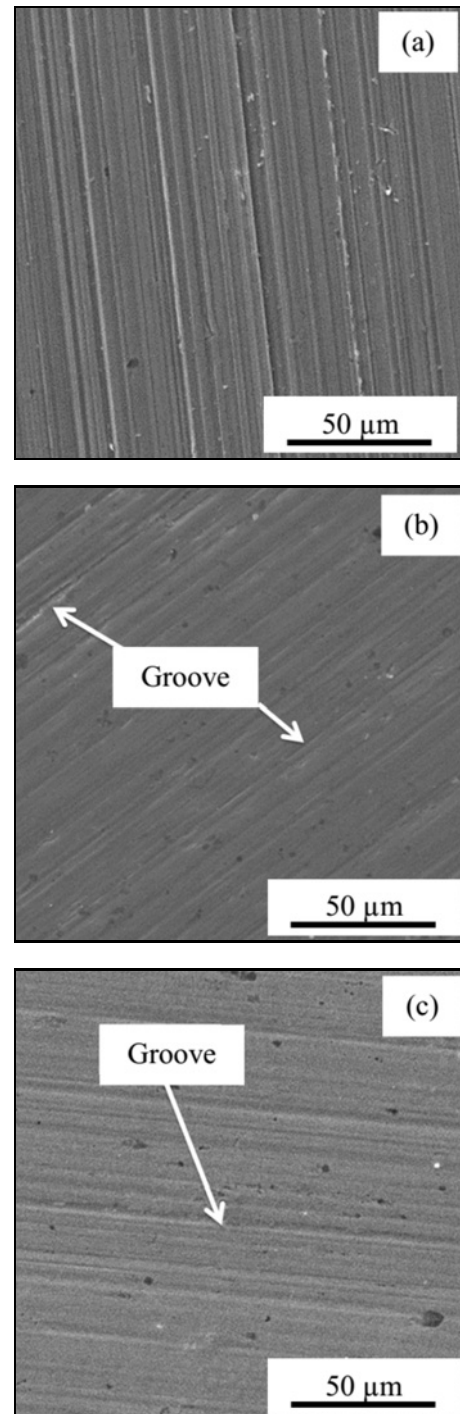


Fig. 14. Surface wear of (a) base metal, (b) sample S2, and (c) sample T2.

lower ductility, which make material less prone to suffer plastic deformation under abrasive wear, material wasting on the surface of samples S2 and T2 was less than on the substrate. The lower weight loss of sample T2 as compared to sample S2 was also due to the high average hardness of sample T2 than sample S2, which increased the wear resistance of the surface of

this sample. Also, owing to particle bonding to the matrix and no indication of brittle failure, no wear debris of TiB₂ and TiC was found on the surface of the coated layer. It seems that ceramic particles have good bonding strength with the matrix, and do not easily pull out from the matrix during wear test.

Figure 14 shows the surface area of the wear samples. As it can be seen, the plastic deformation was modified through the cutting mechanism as well as the formation of the wedge at the edges of the grooves. Such mechanisms have been reported previously [29]. In these types of mechanisms, abrasive particles usually sink in the softness of the matrix, and by moving the counterface plate, it leads to the creation of grooves in which their edges appear in plastic deformation and sometimes in the form of a wedge. The depth and the intensity of the groove and wedge formations depend on the physical shape and the hardness of the abrasive particle as well as the hardness and the microstructure of the sample. The grooves created on the surface of the coated layer are marked with an arrow in Figs. 14b,c. Therefore, with regard to the appearance of the surfaces, it can be concluded that the dominant mechanism for wearing, in this case, was plowing [27].

5. Conclusions

The present study investigated TiC-Al₂O₃ and TiB₂-TiC-Al₂O₃ composite coatings in-situ to improve the wear resistance and hardness of AISI304 stainless steel via the GTAW process. The research findings showed that:

1. The microstructure morphology of the coatings in the weld center, due to the high cooling rate, was lathy δ -ferrite and the microstructure had changed to the skeletal δ -ferrite near the substrate with the decrease in the cooling rate.

2. Cubic titanium carbide particles formed inhomogeneously on Al₂O₃ particles or spontaneously in the austenitic matrix of the 304 stainless steel.

3. In all the coated samples, hardness was increased due to the formation of the composite coatings. However, among the coated specimens, the most optimal mode of coating parameters in terms of hardness and wear resistance for 3TiO₂-4Al-3C and 3TiO₂-4Al-B₄C mixtures was obtained with a heat input of 1.9 kJ mm⁻¹.

4. The formation of reinforcing particles in both the layers of 3TiO₂-4Al-3C and 3TiO₂-4Al-B₄C mixtures resulted in the increase in the wear resistance of the surface up to 2.5 in comparison to that of the substrate.

References

- [1] Buytoz, S., Ulutan, M.: Surface and Coatings Technology, 200, 2006, p. 3698. doi:10.1016/j.surfcoat.2005.02.178
- [2] Curiel, F. F., García, R., López, V. H., González-Sánchez, J.: Corrosion Science, 53, 2011, p. 2393. doi:10.1016/j.corsci.2011.03.022
- [3] Masanta, M., Shariff, S. M., Roy Choudhury, A.: Wear, 271, 2011, p. 1124. doi:10.1016/j.wear.2011.05.009
- [4] Wang, X. H., Song, S. L., Zou, Z. D., Qu, S. Y.: Materials Science and Engineering A, 441, 2006, p. 60. doi:10.1016/j.msea.2006.06.015
- [5] Hamed, M. J., Torkamany, M. J., Sabbaghzadeh, J.: Optics and Lasers in Engineering, 49, 2011, p. 557. doi:10.1016/j.optlaseng.2010.12.002
- [6] Wang, X. H., Zou, Z. D., Qu, S. Y., Song, S. L.: Journal of Materials Processing Technology, 168, 2005, p. 89. doi:10.1016/j.jmatprotec.2004.11.001
- [7] Lin, Y.-C., Chen, H.-M., Chen, Y.-C.: Materials & Design, 47, 2013, p. 828. doi:10.1016/j.matdes.2013.01.007
- [8] Sharifitabar, M., Vahdati Khaki, J., Haddad Sabzevar, M.: Surface and Coatings Technology, 285, 2016, p. 47. doi:10.1016/j.surfcoat.2015.11.019
- [9] Wang, X. H., Zhang, M., Du, B. S.: Tribology Letters, 41, 2011, p. 171. doi:10.1007/s11249-010-9701-6
- [10] Hou, Q. Y.: Surface and Coatings Technology, 226, 2013, p. 113. doi:10.1016/j.surfcoat.2013.03.043
- [11] Zou, B., Shen, P., Cao, X., Jiang, Q.: International Journal of Refractory Metals and Hard Materials, 29, 2011, p. 591. doi:10.1016/j.ijrmhm.2011.04.001
- [12] Mridha, S., Baker, T. N.: Materials Science and Technology, 31, 2015, p. 337. doi:10.1179/1743284714Y.0000000530
- [13] Chatterjee, S., Shariff, S. M., Datta Majumdar, J., Roy Choudhury, A.: The International Journal of Advanced Manufacturing Technology, 38, 2008, p. 938. doi:10.1007/s00170-007-1143-4
- [14] Nam, S., Kim, C., Kim, Y.-M.: Surface and Coatings Technology, 354, 2018, p. 1. doi:10.1016/j.surfcoat.2018.09.012
- [15] Lippold, J. C., Kotecki, D. J.: Welding Metallurgy and Weldability of Stainless Steels. Hoboken, Wiley-Interscience 2005. ISBN 0-471-473-79-0
- [16] Sharifitabar, M., Khaki, J. V., Sabzevar, M. H.: International Journal of Minerals, Metallurgy, and Materials, 23, 2016, p. 193. doi:10.1007/s12613-016-1227-y
- [17] Masanta, M., Shariff, S. M., Roy Choudhury, A.: Materials & Design, 90, 2016, p. 307. doi:10.1016/j.matdes.2015.10.135
- [18] Cai, Y., Luo, Z., Chen, Y., Ao, S.: Surface Engineering, 33, 2017, p. 936. doi:10.1080/02670844.2017.1309742
- [19] Merzhanov, A. G.: Advanced Materials, 4, 1992, p. 294. doi:10.1002/adma.19920040412
- [20] Kumar, S., Shahi, A. S.: Materials & Design, 32, 2011, p. 3617. doi:10.1016/j.matdes.2011.02.017
- [21] Mirshekari, G. R., Tavakoli, E., Atapour, M., Sadeghian, B.: Materials & Design, 55, 2014, p. 905. doi:10.1016/j.matdes.2013.10.064
- [22] Kou, S.: Welding Metallurgy. Hoboken, Wiley-Interscience 2003. ISBN-10: 9780471434917
- [23] Bowen, C. R., Derby, B.: Journal of Materials Science, 31, 1996, p. 3791. doi:10.1007/BF00352794
- [24] Chen, Y., Wang, H. M.: Materials Letters, 57, 2003, p. 1233. doi:10.1016/S0167-577X(02)00964-3

- [25] Wang, X., Zhang, M., Qu, S.: Optics and Lasers in Engineering, 48, 2010, p. 893. [doi:10.1016/j.optlaseng.2010.03.017](https://doi.org/10.1016/j.optlaseng.2010.03.017)
- [26] Vallauri, D., Atías Adrián, I. C., Chrysanthou, A.: Journal of the European Ceramic Society, 28, 2008, p. 1697. [doi:10.1016/j.jeurceramsoc.2007.11.011](https://doi.org/10.1016/j.jeurceramsoc.2007.11.011)
- [27] Akhtar, F.: Journal of Alloys and Compounds, 459, 2008, p. 491. [doi:10.1016/j.jallcom.2007.05.018](https://doi.org/10.1016/j.jallcom.2007.05.018)
- [28] Yilmaz, S. O., Ozenbas, M., Yaz, M.: Tribology International, 42, 2009, p. 1220. [doi:10.1016/j.triboint.2009.04.041](https://doi.org/10.1016/j.triboint.2009.04.041)
- [29] De Pellegrin, D. V., Torrance, A. A., Haran, E.: Wear, 266, 2009, p. 13. [doi:10.1016/j.wear.2008.05.015](https://doi.org/10.1016/j.wear.2008.05.015)